Modulation of Single-Walled Carbon Nanotube Photoluminescence by Hydrogel Swelling

Paul W. Barone, Hyeonseok Yoon, René Ortiz-García, Jingqing Zhang, Jin-Ho Ahn, Jong-Ho Kim, and Michael S. Strano*

Department of Chemical Engineering, Massachusetts Institute of Technology, 77 Massachusetts Avenue, Cambridge, Massachusetts 02139-4307

ABSTRACT We demonstrate the use of hydrogel swelling as a mechanism to reversibly induce solvatochromic shifting in single-walled carbon nanotube (SWNT) near-infrared emission within a biocompatible hydrogel. The optical sensor reports the degree of the swelled state and glucose concentration when apo-glucose oxidase is used to cross-link the hydrogel. Photoluminescence emission maxima from dispersed nanotubes in a poly(vinyl alcohol) hydrogel shift as cross-linking is increased, with a maximum of −48 meV for the (6,5) nanotube. The Raman tangential mode also red shifts up to 17 cm^{-1}, indicative of nanotube lattice strain equivalent to an effective hydrostatic pressure of 3 GPa. While the electronic band gaps of SWNTs are known to either increase or decrease with uniaxial strain or lattice deformation depending on chiral vector, we show that the mechanism of detection is counterintuitively non-strain-dependent. Instead, the data are well-described by a model that accounts for changes in dielectric screening of the 1-D exciton, as the osmotic pressure forces conformational distortions in the PVA by rotating more polar groups to the nanotube surface. The model describes observed changes with hydration state and cross-linking density variation from 0 to 14%. Cross-linking with apo-glucose oxidase renders the hydrogel glucose responsive, and we demonstrate rapid and reversible detection of glucose from these systems after repeated cycling of 10 mM glucose. We also demonstrate detection and imaging in the near-infrared of implanted hydrogel sensors in a mouse tissue model, showing excellent signal-to-noise of 8.6 and contrast with integration times of 60 s.

KEYWORDS: hydrogel · single-walled carbon nanotube · photoluminescence · near-infrared · glucose sensor

Individually dispersed, semiconducting single-walled carbon nanotubes (SWNT)[1,2] and their metallic free bundles exhibit near-infrared (nIR) photoluminescence (PL).[3,4] Previously, we have demonstrated the selective modulation of SWNT PL in response to glucose,[5−7] divalent metal cations,[8] DNA hybridization,[9,10] and reactive oxygen species.[11] The use of SWNTs as nIR optical sensors has potential utility in clinical or medical settings because nanotube PL occurs in a region of the electromagnetic spectrum in which blood and tissue is particularly transparent.[6,12] Additionally, SWNTs do not photobleach[6] and are ideally suited for long-term sensing applications. Hydrogels are cross-linked polymer matrices that can swell in the presence of water and are attractive materials for biological applications due to their biocompatibility and structural properties. They have been proposed as scaffolds for tissue engineering[13−15] and have been fabricated to respond, by expanding or contracting, to specific stimuli for a number of drug delivery[16,17] and sensing applications.[18] Hydrogels have previously been fabricated with single-walled[19−24] and multiwalled[25−27] carbon nanotubes embedded; however, to our knowledge, there exists no demonstration and study of SWNT PL inside a hydrogel matrix. A hydrogel-based sensor utilizing SWNTs would be advantageous for *in vivo* applications due to the inherent biocompatibility of the hydrogel matrix, and if the matrix is nonbiodegradable, it would also prevent nanotube leaching.

Hydrogel swelling is caused by an osmotic pressure in its interior.[28] The osmotic pressure is directly related to the interaction between the polymer and the solvent and the number of cross-links in the hydrogel. For nonionic hydrogels, the total internal osmotic pressure arises from two contributions: osmotic pressure due to mixing and osmotic pressure due to polymer elasticity, with the total osmotic pressure driving hydrogel swelling given by

$$\pi = -\frac{RT}{V_1}\left[(\ln(1-\phi)+\phi+\chi\phi^2)+\frac{1}{N_c}(\phi^{1/3}\phi_0^{2/3}-\phi/2)\right] \quad (1)$$

where R is the universal gas constant, T is the temperature, V_1 is the molar volume of the solvent, χ is the polymer−solvent interaction parameter, ϕ is the polymer volume fraction, ϕ_0 is the polymer volume fraction in the relaxed state, and N_c is the average number of monomers between cross-links.

*Address correspondence to strano@mit.edu.

Received for review August 17, 2009 and accepted November 18, 2009.

Published online November 24, 2009.
10.1021/nn901025x

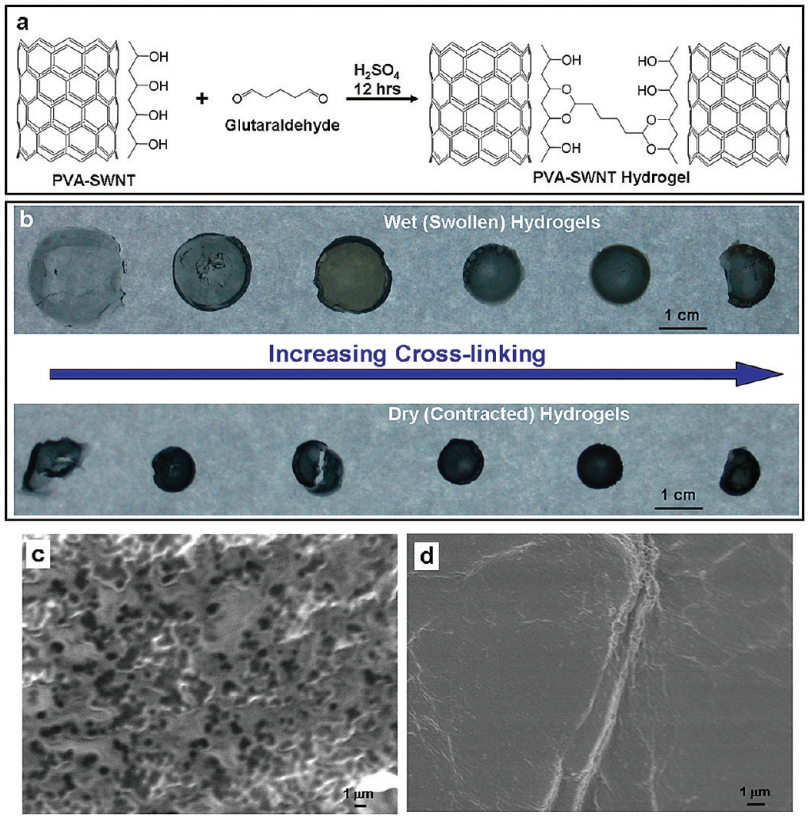

Figure 1. Micrographs of PVA−SWNT hydrogels. (a) Schematic of hydrogel formation using glutaraldehyde as the cross-linker. (b) Poly(vinyl alcohol) hydrogels of different cross-linking densities with individually dispersed single-walled carbon nanotubes embedded inside. The lowest cross-linked hydrogels show the largest volume change upon swelling with water. (c,d) Scanning electron microscopy shows visible pores in the hydrogel at the lowest cross-linking (c) while the highest cross-linked hydrogels have no visible pore structure (d).

At equilibrium, the elastic and mixing osmotic pressures cancel, and the total osmotic pressure is equal to zero. Changing the cross-linking density also changes N_c and the elastic osmotic pressure. Single-walled carbon nanotube emission energy has been shown, both theoretically[29,30] and experimentally,[31] to shift in response to lattice deformation, such as that experienced under hydrostatic pressure. In the case of uniaxial strain, the sign of emission shift is opposite for mod($n-m$,3) = 2 and mod($n-m$,3) = 1 nanotubes. However, SWNT PL is also sensitive to the local environment and will shift in response to changes in the local dielectric properties.[32,33]

Here we report shifts in emission from SWNT hydrogel composites by embedding SWNTs inside a poly(vinyl alcohol) (PVA) hydrogel. As the cross-linking density and hydration state of the hydrogel are changed, the SWNT Raman scattering G-band upshifts, indicating deformation of the nanotube lattice, while the SWNT PL also decreases in energy. However, strain-induced effects are not sufficient to describe the observed PL shift. Instead, we describe and model a new mechanism where hydrogel cross-linking density and internal pressure induce changes in the local dielectric around the nanotube, causing the nanotube PL to shift. The developed model shows good agreement between hydrogels in the dry and wet state and as a function of N_c^{-1}.

To embed nanotubes inside a PVA hydrogel, we first suspended SWNTs in PVA. Nanotubes from Southwest Nanotechnologies were suspended in a 2 wt % sodium cholate solution,[4] which was further purified and enriched in the (6,5) nanotube using density gradient centrifugation.[34] The resulting solutions were mixed with PVA dissolved in water to give a final PVA concentration of 5 wt % and then dialyzed against surfactant-free buffer.[5] To the PVA-suspended nanotubes were added varying amounts of glutaraldehyde as the cross-linking agent, followed by H_2SO_4 as the catalyst (Figure 1a).[35] The solutions were mixed well and then poured into Teflon molds and allowed to set for 12 h. The hydrogels were then washed with water until the pH of the solution was neutral and dried under vacuum until the weight of the hydrogels was constant. Figure 1b is a picture of SWNT−PVA hydrogels with six different cross-linking densities ranging from N_c^{-1} = 0.003 to N_c^{-1} = 0.123 in the swollen and dried state. Here we choose to use N_c^{-1}, which is the inverse of the average number of monomers between cross-links and is unitless, as a measure of hydrogel cross-linking. For simplicity, we have assumed that all of the glutaraldehyde has reacted to form cross-links within the hydrogel. The size of the hydrogel decreases with increasing cross-linking for hydrogels in the wet state. The hydrogel with the lowest cross-linking density shows the largest volume change upon swelling, as expected,[28] and is the most deformed in the dry state. Scanning electron micrographs of the dried hydrogel (Figure 1c,d) show significant differences in the microstructure of the gel as the cross-linking is increased. Hydrogels with lower cross-linking densities have visible pores in the gel structure (Figure 1c), while higher cross-linked hydrogels have no visible pore structure and appear as a continuous surface (Figure 1d).

Raman scattering frequencies from SWNTs inside the hydrogel upshift with increasing hydrogel cross-linking densities and hydration state. Figure 2a shows the Raman G-band at 785 nm excitation from wet hydrogels with cross-linking densities of N_c^{-1} = 0.003 and N_c^{-1} = 0.123. There is a 4 cm^{-1} upshift as cross-linking is increased for the G-bands shown in Figure 2a. A similar shift is seen for hydrogels in the dry state, with a maximum shift of almost 17 cm^{-1} observed. A plot of the shift in Raman frequency, normalized by the PVA−SWNT solution G-band frequency (shown as

$(\omega - \omega_0)/\omega_0$), *versus* cross-linking is shown in Figure 2b. Shifts in Raman frequency of the G-band for SWNT can occur due to deformation of the SWNT lattice structure,[36,37] where strain in the lattice can result in either a lengthening or shortening of the carbon−carbon bond. From the theoretical treatment of Reich *et al.*, we conclude that the upshift in frequency observed here is due to a shortening of the carbon−carbon bond as though the nanotube is experiencing a hydrostatic pressure.[36] Using the relation of 3.8 GPa/frequency shift,[36] we calculate an effective pressure felt by the carbon nanotube, shown on the right axis in Figure 2b. There is further shifting of the G-band frequency as the hydrogel is dried. For a hydrogel with the $N_c^{-1} = 0.123$, a shift of 14 cm^{-1} is observed as the hydrogel goes from wet to dry (Figure 2c) and is equivalent to 2.3 GPa. Note the linear dependence *versus* N_c^{-1} is predicted by rubber elasticity theory.

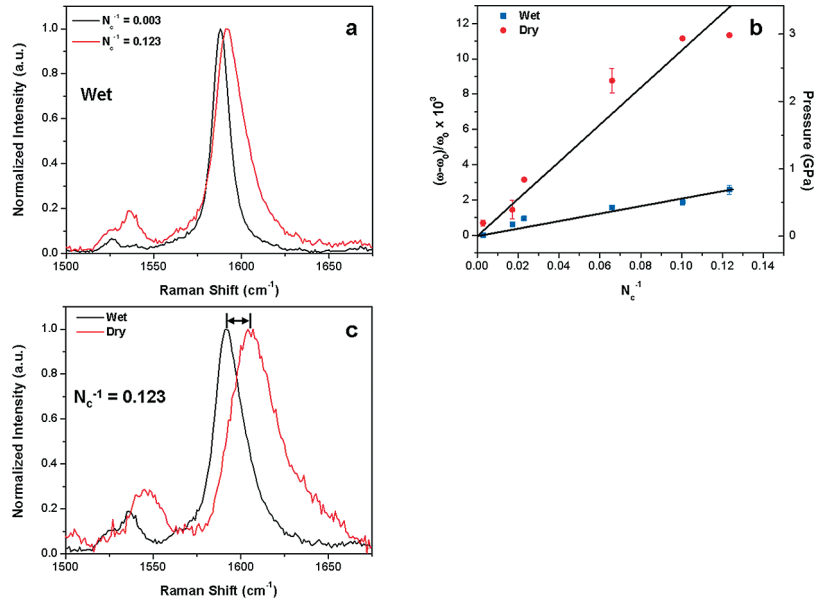

Figure 2. Nanotube Raman shifts with increasing hydrogel cross-linking and hydration. (a) G-band of SWNT shows a shift in frequency as the hydrogel cross-linking is increased, shown for hydrogels in the wet state. (b) Shift in frequency is largest for the hydrogels in the dry state with a maximum shift of 17 cm^{-1} when compared to a PVA−SWNT solution. In contrast, the wet hydrogels show a maximum shift of only 4 cm^{-1}. Lines highlight the linear nature of pressure *vs* N_c^{-1}. (c) Raman G-band is also shown to upshift when the hydrogel is in the dried state, with the maximum shift in Raman frequency of 14.7 cm^{-1}. The right axis of (b) shows the calculated pressure felt by the nanotube assuming a 3.8 cm^{-1} shift per GPa.

The photoluminescence emission maxima from the SWNT−PVA hydrogels also shift depending on hydrogel cross-linking and hydration state. Nanotube emission spectra were measured using an InGaAs array coupled to an inverted Zeiss microscope. Figure 3a shows excitation−emission profiles for the PVA−SWNT hydrogels at cross-linking densities of $N_c^{-1} = 0.003$ and $N_c^{-1} = 0.123$ inside wet hydrogels. As the cross-linking density is increased, there is a clear red shift in the PL emission maxima for all three nanotubes. A similar trend is observed for hydrogels in the dry state (Figure 3b). Previous work by Tan and Torrens has demonstrated exciton energy transfer between adjacent semiconducting nanotubes.[38,39] Since the (8,3) nanotube has the largest band gap of the nanotubes in the sample, changes in the nanotube−nanotube distance, due to increases in the hydrogel cross-linking density or drying the hydrogel, result in energy transfer from the (8,3) nanotube to either the (7,5) or the (6,5) nanotubes (Figure 3c,d), which can be seen as a decrease in the (8,3) PL intensity relative to intensities of the (6,5) and (7,5) nanotubes. Figure 3a,b also shows significant broadening of SWNT PL as cross-linking is increased and the hydrogel is dried. We attribute this to heterogeneous peak broadening due to inhomogeneous environments seen by all of the nanotubes in the hydrogel. We assert that this inhomogeneity is localized to the nanotube itself as different spatial locations on the hydrogel did not show location-specific emission maxima. Plotting the emission peak center *versus* cross-linking shows an apparently linear decrease in emission energy for the (6,5), (7,5), and (8,3) nanotubes in wet hydrogels (Figure 3e−g). For the (6,5) and (7,5) nanotubes, the shift in emission maxima in the dry hydrogel appears to reach a saturation point where further cross-linking of the hydrogel will not cause further shifting. While the emission maximum generally decreases with increasing cross-linking for the (8,3) nanotube in a dry hydrogel, there is significant scatter of the data points. We attribute this to the broadening and energy transfer observed in the spectra, making exact emission maxima identification difficult.

The band gap of nanotubes experiencing lattice deformation will either increase or decrease depending on the strain and the nanotube type.[29,30] From Gartstein *et al.*, we get the shift in band gap with radial, η_r, and axial, η_z, strain for the E_{11} gap

$$\Delta E_{strain} = -2E_{11}\eta_r + 3\gamma_0(-1)^q(\eta_r - \eta_z)\cos(3\theta) \quad (2)$$

where, E_{11} is the band gap in vacuum, γ_0 is the nearest neighbor electron hopping parameter and ranges from 2.4 to 2.9 eV, q is equal to mod($n-m$,3), and θ is the nanotube chiral angle. The radial and axial strain is nanotube-dependent, and we can estimate them using the relations of Capaz *et al.* with the pressure estimates from before.[40] For γ_0, we chose to use 2.54 eV measured by Leeuw recently for nanotubes under uniaxial strain,[31] although using another value for γ_0 leads to only minimal changes in the results. Figure 3h−j plots the shift in SWNT PL peak center *versus* cross-linking for the dry to wet hydrogel transition as well as the calculated shift due to strain. For all three nanotube species, the change in band gap due to strain

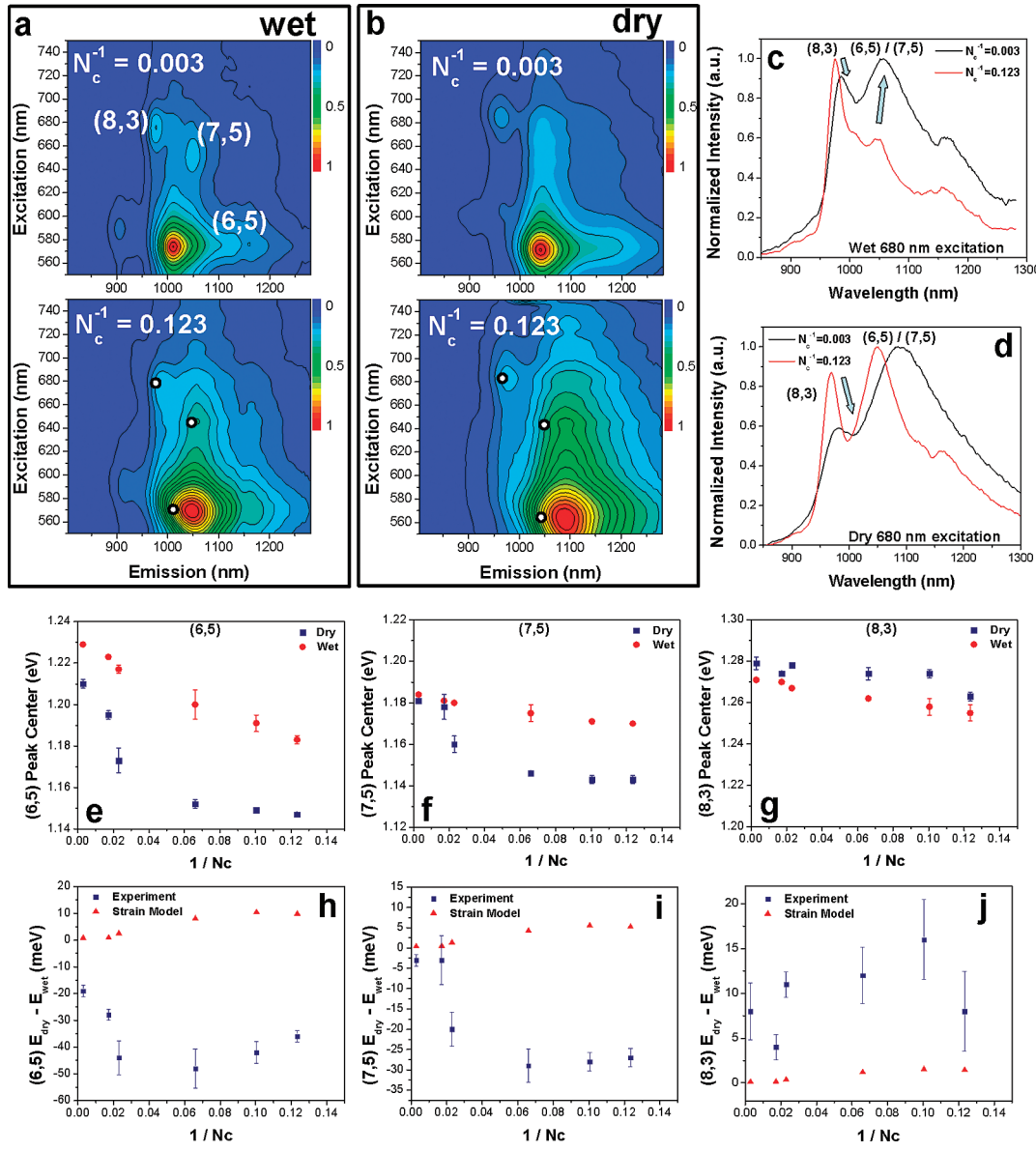

Figure 3. Nanotube fluorescence decreases in energy as hydrogel cross-linking increases. (a) SWNT photoluminescence red shifts as the hydrogel cross-linking is increased for the (6,5), (7,5), and (8,3) nanotubes in wet hydrogels (in a). The maximum shift observed in these experiments is from the (6,5) nanotube, with a shift of −48 meV. (b) A similar trend is observed for nanotubes in dry hydrogels for the (6,5), (7,5), and (8,3) nanotubes. In (a) and (b), white dots show nanotube peak centers in hydrogels with $N_c^{-1} = 0.003$. (c,d) Photoluminescence spectra of hydrogels with excitation in resonance with the (8,3) nanotube for $N_c^{-1} = 0.003$ and 0.123 in the wet (c) and dry (d) state. There is clear energy transfer from the (8,3) nanotube to the (6,5) and (7,5) nanotubes. (e−g) For all three nanotube species, the photoluminescence red shift plotted *versus* N_c^{-1} appears to be linear when the hydrogels are wet. When the hydrogels are dry, the shift in photoluminescence appears to reach a plateau for both the (6,5) and the (7,5) nanotube (e and f). In the case of the (8,3) nanotube, this is not the case, and the shift with cross-linking appears to follow a similar slope as the wet hydrogel. (h−j) Plots of the shifts of SWNT PL from the wet to the dry state (squares) and the modeled shifts due to strain (triangles).

effects is unable to explain the observed shift in SWNT PL. For both the (6,5) and (7,5) nanotubes, the predicted shift due to strain is of the opposite sign as the observed shift. In the case of the (8,3) nanotube, the sign of the shift is correct, but the magnitude is insufficient. We therefore conclude that strain alone cannot explain the observed shifts and is not the dominant factor.

As nanotube lattice deformation is unable to describe the observed shift, we explored several alternative hypotheses. As seen in Figure 3c,d, there is exciton energy transfer between the nanotubes in the hydrogel. It is possible that part of the large shift in PL for the (6,5) nanotube is, in part, due to exciton-energy transfer to the (7,5) nanotube. This effect is expected to be very sensitive to the nanotube loading in the hydrogel, with lower loading leading to decreased energy transfer because the SWNT spacing would become too large for such effects to be prominent. However, decreasing the nanotube loading by an order of magni-

tude does not change the shift of the nanotube fluorescence (Figure S1 in Supporting Information).

We explored the possibility that SWNT length, which affects the intertube distance, contributes to the shift. In the case of long nanotubes, it is conceivable that they could be exposed to greater strain along the length of the nanotube due to polymer entanglement, yet changes in nanotube length did not cause any change in the observed shift (Figure S2). Additionally, it is possible that local heating of the nanotube, due to the excitation source, could lead to the observed shift. If heating plays a role, the PL shift would be commensurate for all of the dried hydrogels, but because this is not the case, we reject this possibility.

While it is expected that the local dielectric seen by the nanotube is different between the dry (air) and wet state, changing the cross-linking density, and thus the hydrogel osmotic pressure, could change polymer conformation and therefore the local dielectric constant seen by the nanotube. We have previously put forth a model to describe solvatochromism in SWNTs, but we did not explicitly calculate the dielectric constant for SWNTs in different media.[32] Nanotube PL is excitonic in nature,[41] having strongly bound excitons with an exciton binding energy, E_{bind}, and a self-interaction energy between the excited excitonic states, E_{SI}. Both E_{bind} and E_{SI} will experience screening from the dielectric environment causing their energies to decrease.[33,42] Scaling relations of the exciton binding energy with the dielectric have been found to be $E_{bind} \propto \varepsilon^{-1.4}$ from Perebeinos *et al.* and $E_{bind} \propto \varepsilon^{-1.2}$ from Walsh *et al.* Similarly, the self-interaction energy scales inversely with the dielectric. Therefore, we can relate the shift in emission maxima to changes in the exciton binding energy and the self-interaction energy

$$\Delta E = \Delta E_{SI} - \Delta E_{bind} + \Delta E_{strain} \quad (3)$$

with the change in self-interaction and exciton binding energies given by

$$\Delta E_{SI} = E_{SI}^{\varepsilon=1}\left(\frac{1}{\varepsilon} - 1\right)$$
$$\Delta E_{bind} = E_{bind}^{\varepsilon=1}\left(\frac{1}{\varepsilon^{1.2}} - 1\right) \quad (4)$$

where $E_{SI}^{\varepsilon=1}$ and $E_{bind}^{\varepsilon=1}$ are the self-interaction and exciton binding energies in vacuum, respectively.[33] Using the above model, we tested if a change in dielectric constant could self-consistently model the sign and magnitude of the observed shift for all three nanotubes

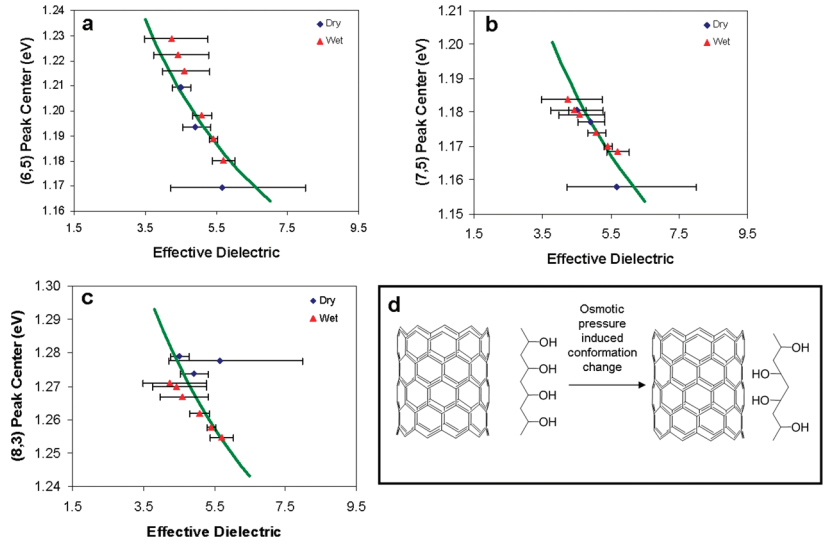

Figure 4. Changes in local dielectric constant due to cross-linking cause nanotube photoluminescence to shift. (a−c) Peak center for the (6,5), (7,5), and (8,3) nanotubes plotted *versus* the calculated dielectric constant using the excitonic model discussed in the text. For the (6,5) and the (7,5) nanotubes, the emission energies collapse onto one continuous line for both the wet (squares) and the dry (diamonds) hydrogels. The values predicted by the model are shown as a solid line. For all three hydrogels, the most cross-linked hydrogels in the dry state are not shown for clarity due to the size of the confidence intervals. (d) Schematic of the possible PVA conformational change due to changes in osmotic pressure and cross-linking.

reported. Here, we use the scaling relation from Walsh *et al.* It is possible to estimate $E_{bind}^{\varepsilon=1}$ using an empirical relation from Capaz *et al.*, who performed *ab initio* modeling to calculate E_{bind}.[43] However, no such relation exists for calculating $E_{SI}^{\varepsilon=1}$. Dukovic *et al.* have directly measured the exciton binding energy for 13 nanotubes in a PMAOVE polymer matrix, including the (6,5), (7,5), and (8,3) nanotubes.[44] Using the relation from Capaz, we estimate the effective dielectric from the PMAOVE matrix and then calculate $E_{SI}^{\varepsilon=1}$. The self-interaction energies calculated from the Dukovic data are 1.903, 1.853, and 1.975 eV for the (6,5), (7,5), and (8,3) nanotubes, respectively, with corresponding exciton binding energies of 1.647, 1.581, and 1.718 eV. Using these values, we fit the data of each hydrogel (six cross-linking densities and two hydration states) using eq 3 by calculating the effective dielectric seen by the nanotube. However, the $E_{SI}^{\varepsilon=1}$ above did not provide an optimal fit, and the following values were used $E_{SI,(6,5)} = 1.954 \pm 0.007$ eV, $E_{SI,(7,5)} = 1.812 \pm 0.005$ eV, and $E_{SI,(8,3)} = 1.963 \pm 0.007$ eV with the listed 99.9% confidence intervals. We note that the new E_{SI} energies are within 3% of the original estimations. The data and the calculated fits for each hydrogel are shown in the Supporting Information (Figures S3 and S4). In fitting the three most cross-linked hydrogels in the dry state, PL data from the (8,3) nanotube were not included because of uncertainty in the actual peak center due to broadening (Figure 3d). Figure 4a−c plots nanotube peak center *versus* the dielectric constant determined from fitting each hydrogel separately, with 95% confidence intervals for each dielectric constant included. The three most cross-

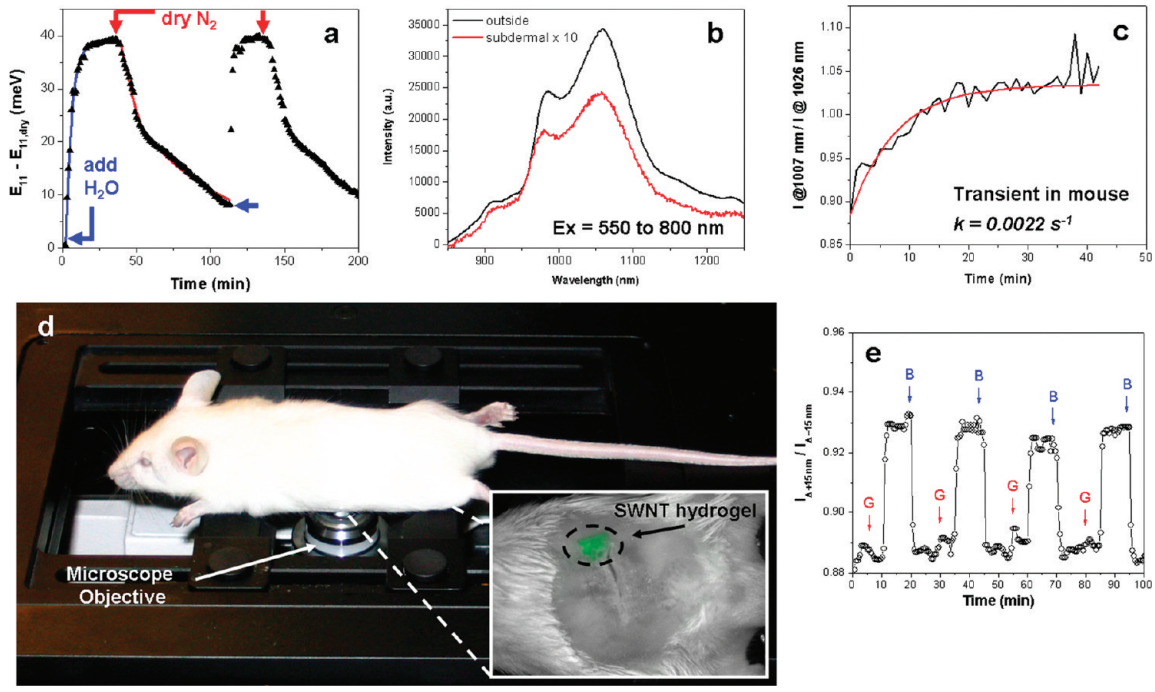

Figure 5. Transient hydrogel expansion and photoluminescence detection inside a mouse. (a) Changing the hydrogel from the wet to dry state causes a reversible shift in fluorescence that can be monitored transiently. For the lowest cross-linked hydrogel, the shift in peak center from wet to dry is reversible and reproducible. A first-order approximation can be used to determine the time constant, with expansion shown in blue and contraction shown in red. (b) Spectra of hydrogels outside of (black) and implanted subdermally inside a mouse (red, ×10) taken using a NIR fluorescence microscope, as shown in (d). (c) Transient shift during hydrogel expansion of SWNT PL for PVA−SWNT hydrogel, with $N_c^{-1} = 0.003$, implanted in a mouse, reported as the intensity at 1007 nm divided by the intensity at 1026 nm with excitation from 550 to 800 nm and a 60 s exposure. Applying the same first-order model as in (a) yields a time constant of 0.0022 s^{-1} and is of the same order as expansion from (a). (d) Picture of measurement setup with mouse positioned on the microscope. Inset shows a fluorescence image of a PVA−SWNT hydrogel implanted subdermally in a mouse and imaged using a CRi-Maestro *in vivo* imager with excitation from 576 to 605 nm and emission from 840 to 950 nm with a 5 s exposure. (e) Responses of apoGOx-attached hydrogel upon periodic exposure to glucose (G: 10 mM glucose; B: 10 mM PBS solution, pH 6.8). The PL shift was monitored by calculating the integrated intensity ratio of emission at ±15 nm ranges from the (6,5) peak center.

linked hydrogels in the dry state are not shown because the confidence intervals are so large as to render them useless. For all three nanotubes, the wet and dry hydrogel data converge to a single line. The calculated dielectrics fall within a reasonable range, and we assume $\varepsilon_{PVA} = 6.9$ (from ref 45), $\varepsilon_{water} = 1.769$ (ref 33), and $\varepsilon_{air} \sim 1$ leading to a fractional PVA coverage on the nanotube of 48 to 79%. From this analysis, we conclude that changing the cross-linking density of the hydrogel, which simultaneously changes the internal osmotic pressure, causes a polymer conformational change on the nanotube surface, forcing free OH groups on the PVA to associate with the nanotube surface (Figure 4d), resulting in a change of the local dielectric and a shift in SWNT emission energy. Finally, we point out that the interfacial contact between the SWNT and the hydrogel is essential to the observation of this phenomenon. It is conceivable that heterogeneities in SWNT−PVA contact area are responsible for broadening of the SWNT PL and for the measured variations in SWNT PL shift.

It is possible to use stimulus responsive hydrogels as sensors and drug delivery vehicles. Figure 5a shows the transient response of a hydrogel with cross-linking $N_c^{-1} = 0.003$ as the hydrogel is swollen and then dried. Both the expansion and contraction can be approximated as two first-order processes, $\Delta E_{Norm} = \exp(-kt)$, with the measured PL shifts normalized to fall between 0 and 1, t the time in seconds, and k the rate constant for the process, with the modeled response shown in Figure 5a. Hydrogel expansion has a $k = 0.004\ s^{-1}$, while hydrogel drying is almost an order of magnitude slower than expansion and has two distinct regions with rate constants of 0.00062 and 0.00025 s^{-1}. As a practical demonstration of sensor operation through thick tissue, a SWNT−hydrogel sensor was implanted subdermally in a deceased mouse. The mouse was euthanized through CO_2 asphyxiation and shaved with the hydrogel inserted between the dermis and the abdominal muscles through a slit cut in the abdominal skin. Figure 5b shows SWNT PL from the same hydrogel outside of the mouse and implanted subdermally, respectively. The experimental setup is pictured in Figure 5d, where the mouse was positioned over the inverted microscope 20× objective. From Figure 5b, it is clear that with 550 to 800 nm excitation it is possible to detect SWNT PL through skin and tissue. Figure 5c demonstrates transient expansion of a hydrogel, with $N_c^{-1} =$

0.003, implanted subdermally (*i.e.*, beneath the skin) in the mouse and swollen with water. The shift is presented as an intensity ratio of emission at 1007 nm, the peak center of the (6,5) nanotube in the wet hydrogel, and 1026 nm, the peak center in the dry hydrogel. As the emission maximum shifts, the reported ratio increases. Applying the same first-order model as in Figure 5a yields a rate constant of 0.0022 s^{-1} and is the same order of magnitude as seen in Figure 5a. From Figure 5c, we calculate a signal-to-noise ratio of 8.6. As a demonstration of the use of the hydrogel platform for sensing, a model glucose sensor was fabricated. Apoglucose oxidase (apoGOx), glucose oxidase without the cofactor, was chemically attached to the PVA hydrogel matrix for selective recognition of glucose. Upon periodic exposure to glucose, as shown in Figure 5e, the apoGOx-attached hydrogel provided a reversible real-time change in PL signal. Since apoGOx contains many lysine residual groups, it can act as a cross-linker to couple adjacent carboxylated PVA chains. Therefore, the apoGOx−glucose interaction can cause changes in interior hydrostatic pressure and PVA chain conformation, resulting in a PL shift *via* the dielectric screening mechanism described above.

In conclusion, we have demonstrated, for the first time, the shift of nanotube photoluminescence in a hydrogel matrix. As the hydrogel cross-linking density and hydration state is changed, the nanotubes experience lattice deformations and a shift in PL emission maxima. However, the lattice deformations alone cannot describe the PL shifts. Instead, we find that changes in the local dielectric around the nanotube are what cause the SWNT PL shifts. Incorporation of SWNTs inside stimuli responsive hydrogels, similar to the glucose version demonstrated in this work, will yield new platforms for *in vivo* detection utilizing the inherent biocompatibility of the hydrogel.

MATERIALS AND METHODS

Materials. Single-walled carbon nanotubes were purchased from Southwest Nanotechnologies and subjected to the purification described below. Sodium cholate, sodium dodecyl sulfate, iodixonal, poly(vinyl alcohol) (85 to 124 kD M_w, 88% hydrolyzed), and glutaraldehyde were purchased from Sigma Aldrich and used as received.

Nanotube Suspension and Purification. Single-walled carbon nanotubes were first suspended in a 2 wt % sodium cholate (SC) aqueous solution using published methods.[4] Nanotubes were mixed with a 2 wt % SC aqueous solution at a concentration of 1 mg/mL and probe tip sonicated, 6 mm tip, at 40% amplitude for 2 h in an ice bath. The solution was centrifuged 4 h at 30 000 rpm in a Beckman ultracentrifuge. The resulting nanotube solution was enriched in the (6,5) nanotube species using a modified density gradient procedure from the literature.[34] Briefly, a SC−SWNT aqueous suspension was mixed with a 2 wt % sodium dodecyl sulfate (SDS) solution to a final ratio of 1:4 SDS/SC. Into a 16.8 mL Beckman ultracentrifuge tube were layered 3 mL of 60% iodixanol, 6 mL of a 30 to 15% iodixanol step gradient, and 4 mL of the SDS/SC suspended SWNT solution. All iodixanol layers contained 2 wt % surfactant in a ratio of 1:4 SDS/SC. The tubes were centrifuged 12 h at 32 000 rpm and 22 °C. After centrifugation, the resulting gradient was fractionated into 250 μL fractions using a Beckman fractionator. Fractions were characterized by UV−vis−nIR absorption and fluorescence and fractions enriched in the (6,5) nanotube species from disparate tubes were combined.

Hydrogel Preparation. Iodixanol from the diameter purification procedure was first removed *via* dialysis, with enriched fractions being dialyzed against a 2 wt % SC solution. A 10 wt % PVA solution was prepared by dissolving the requisite amount of PVA in Milli-Q water at 80 °C. The (6,5)-enriched nanotubes were mixed with the 10% PVA in a 1:1 ratio to give a 5% PVA/SC−SWNT mixture. The PVA was assembled on the nanotube surface, and the free SC was removed *via* dialysis. Hydrogels were then prepared by taking 1 mL of the PVA−SWNT solution adding glutaraldehyde, as the cross-linker, followed by 0.1 M H_2SO_4, as the catalyst. The solution was poured into a Teflon mold and allowed to set overnight. After gelation, the hydrogels were rinsed with Milli-Q water until pH was constant and then dried under vacuum.

Measure SWNT Raman and Photoluminescence. Nanotube Raman scattering was collected with a Kaiser Raman RXN system with a 785 nm laser photodiode, 30 mW at the source, with 1 s exposure and 5 accumulations. Nanotube photoluminescence from the hydrogels was measured using a home-built near-infrared PL microscope. Briefly, a Zeiss AxioVision inverted microscope with a 20× objective was coupled to a Princeton Instruments InGaAs 1-D array detector through a PI-Acton SP150 spectrograph. A white light excitation source coupled to a monochromator was used for excitation light. For broad-band excitation from 550 to 800 nm, the fluence at the sample was <2500 mW/cm^2.

Measuring SWNT PL Inside Mouse. A male mouse was first asphyxiated using CO_2. The mouse was then shaved to remove excess fur, and a small slit was cut into the skin, being careful not to puncture the peritoneum. The hydrogel was inserted into the slit, and the mouse was placed belly side down on a glass coverslip. Through a 20× objective, the surface of the mouse skin was brought into focus and nanotube spectra were taken with the same microscope apparatus as described above with excitation from 550 to 800 nm and a 60 s exposure time. Emission was collected from 850 to 1250 nm.

Acknowledgment. This work was funded by the National Science Foundation and the Beckman Young Investigator Award to M.S.S. P.W.B. received funding from the School of Chemical Sciences at UIUC in the form of a Drickamer Graduate Fellowship. H.Y. was partially supported by the Korea Research Foundation Grant funded by the Korean Government (KRF-2008-357-D00080). The authors would like to thank J.H. Choi and N. Nair for helpful discussions. The authors would also like to thank K. Schlieper, D. Schauer, L.J. Trudel, S.R. Tannenbaum, and G.N. Wogan for help with the mouse experiments.

Supporting Information Available: Shift of (6,5) and (7,5) nanotube emission *versus* nanotube loading (Figure S1), shift of (6,5) emission *versus* nanotube length (Figure S2), measured and calculated peak centers for the (6,5), (7,5), and (8,3) hydrogels (Figures S3 and S4), fit of hydrogel expansion to first-order rate model (Figure S5), scheme for glucose sensitive hydrogel fabrication (Figure S6), method for synthesis of apoGOx (Figures S7−S9), FTIR and Coomassie brilliant blue staining of apoGOx-immobilized PVA−SWNT hydrogels (Figures S10 and S11), schematic of continuous glucose detection setup (Figure S12), and control response of PVA−SWNT hydrogel to glucose (Figure S13). This material is available free of charge *via* the Internet at http://pubs.acs.org.

REFERENCES AND NOTES

1. Reich, S.; Thomsen, C.; Maultzsch, J. *Carbon Nanotubes-Basic Concepts and Physical Properties*; Wiley-VCH: Weinheim, Germany, 2004.

2. Saito, R.; Dresselhaus, M. S.; Dresselhaus, G. *Physical Properties of Carbon Nanotubes*; Imperial College Press: London, 1998.
3. Bachilo, S. M.; Strano, M. S.; Kittrell, C.; Hauge, R. H.; Smalley, R. E.; Weisman, R. B. Structure-Assigned Optical Spectra of Single-Walled Carbon Nanotubes. *Science* **2002**, *298*, 2361–2366.
4. O'Connell, M. J.; Bachilo, S. M.; Huffman, C. B.; Moore, V. C.; Strano, M. S.; Haroz, E. H.; Rialon, K. L.; Boul, P. J.; Noon, W. H.; Kittrell, C.; *et al.* Band Gap Fluorescence from Individual Single-Walled Carbon Nanotubes. *Science* **2002**, *297*, 593–596.
5. Barone, P. W.; Baik, S.; Heller, D. A.; Strano, M. S. Near-Infrared Optical Sensors Based on Single-Walled Carbon Nanotubes. *Nat. Mater.* **2005**, *4*, 86–92.
6. Barone, P. W.; Parker, R. S.; Strano, M. S. *In Vivo*Fluorescence Detection of Glucose Using a Single-Walled Carbon Nanotube Optical Sensor: Design, Fluorophore Properties, Advantages, and Disadvantages. *Anal. Chem.* **2005**, *77*, 7556–7562.
7. Barone, P. W.; Strano, M. S. Reversible Control of Carbon Nanotube Aggregation for a Glucose Affinity Sensor. *Angew. Chem., Int. Ed.* **2006**, *45*, 8138–8141.
8. Heller, D. A.; Jeng, E. S.; Yeung, T. K.; Martinez, B. M.; Moll, A. E.; Gastala, J. B.; Strano, M. S. Optical Detection of DNA Conformational Polymorphism on Single-Walled Carbon Nanotubes. *Science* **2006**, *311*, 508–511.
9. Jeng, E. S.; Barone, P. W.; Nelson, J. D.; Strano, M. S. Hybridization Kinetics and Thermodynamics of DNA Adsorbed to Individually Dispersed Single-Walled Carbon Nanotubes. *Small* **2007**, *3*, 1602–1609.
10. Jeng, E. S.; Moll, A. E.; Roy, A. C.; Gastala, J. B.; Strano, M. S. Detection of DNA Hybridization Using the Near-Infrared Band-Gap Fluorescence of Single-Walled Carbon Nanotubes. *Nano Lett.* **2006**, *6*, 371–375.
11. Heller, D. A.; Jin, H.; Martinez, B. M.; Miller, B. M.; Patel, D.; Yeung, T. K.; Jena, P. V.; Hobartner, C.; Ha, T. J.; Silverman, S. K.; *et al.* Multi-Modal Optical Sensing and Analyte Specificity *via* Single Walled Carbon Nanotubes. *Nat. Nanotechnol.* **2009**, *4*, 114–120.
12. Wray, S.; Cope, M.; Delpy, D. T.; Wyatt, J. S.; Reynolds, E. O. R. Characterization of the Near-Infrared Absorption-Spectra of Cytochrome-Aa3 and Hemoglobin for the Non-Invasive Monitoring of Cerebral Oxygenation. *Biochim. Biophys. Acta* **1988**, *933*, 184–192.
13. Mann, B. K.; Gobin, A. S.; Tsai, A. T.; Schmedlen, R. H.; West, J. L. Smooth Muscle Cell Growth in Photopolymerized Hydrogels with Cell Adhesive and Proteolytically Degradable Domains: Synthetic Ecm Analogs for Tissue Engineering. *Biomaterials* **2001**, *22*, 3045–3051.
14. Ford, M. C.; Bertram, J. P.; Hynes, S. R.; Michaud, M.; Li, Q.; Young, M.; Segal, S. S.; Madri, J. A.; Lavik, E. B. A Macroporous Hydrogel for the Coculture of Neural Progenitor and Endothelial Cells to Form Functional Vascular Networks *In Vivo*. *Proc. Natl. Acad. Sci. U.S.A.* **2006**, *103*, 2512–2517.
15. Lee, M. K.; Bae, Y. H. Cell Transplantation for Endocrine Disorders. *Adv. Drug Delivery Rev.* **2000**, *42*, 103–120.
16. Podual, K.; Doyle, F. J.; Peppas, N. A. Dynamic Behavior of Glucose Oxidase-Containing Microparticles of Poly(ethylene glycol)-Grafted Cationic Hydrogels in an Environment of Changing pH. *Biomaterials* **2000**, *21*, 1439–1450.
17. Podual, K.; Doyle, F. J.; Peppas, N. A. Glucose-Sensitivity of Glucose Oxidase-Containing Cationic Copolymer Hydrogels Having Poly(ethylene glycol) Grafts. *J. Controlled Release* **2000**, *67*, 9–17.
18. Miyata, T.; Asami, N.; Uragami, T. Preparation of an Antigen-Sensitive Hydrogel Using Antigen−Antibody Bindings. *Macromolecules* **1999**, *32*, 2082–2084.
19. Bhattacharyya, S.; Guillott, S.; Dabboue, H.; Tranchant, J. F.; Salvetat, J. P. Carbon Nanotubes as Structural Nanofibers for Hyaluronic Acid Hydrogel Scaffolds. *Biomacromolecules* **2008**, *9*, 505–509.
20. Lachman, N.; Bartholome, C.; Miaudet, P.; Maugey, M.; Poulin, P.; Wagner, H. D. Raman Response of Carbon Nanotube/PVA Fibers under Strain. *J. Phys. Chem. C* **2009**, *113*, 4751–4754.
21. Liu, L. Q.; Barber, A. H.; Nuriel, S.; Wagner, H. D. Mechanical Properties of Functionalized Single-Walled Carbon-Nanotube/Poly(vinyl alcohol) Nanocomposites. *Adv. Funct. Mater.* **2005**, *15*, 975–980.
22. MacDonald, R. A.; Voge, C. M.; Kariolis, M.; Stegemann, J. P. Carbon Nanotubes Increase the Electrical Conductivity of Fibroblast-Seeded Collagen Hydrogels. *Acta Biomater.* **2008**, *4*, 1583–1592.
23. Ogoshi, T.; Takashima, Y.; Yamaguchi, H.; Harada, A. Chemically-Responsive Sol−Gel Transition of Supramolecular Single-Walled Carbon Nanotubes (Swnts) Hydrogel Made by Hybrids of Swnts and Cyclodextrins. *J. Am. Chem. Soc.* **2007**, *129*, 4878–4879.
24. Wang, Z. M.; Chen, Y. M. Supramolecular Hydrogels Hybridized with Single-Walled Carbon Nanotubes. *Macromolecules* **2007**, *40*, 3402–3407.
25. Liu, Z. Q.; Luo, Y. L.; Zhang, K. P. P(Aam-Co-Maa) Semi-Ipn Hybrid Hydrogels in the Presence of Pani and MWNTs-COOH: Improved Swelling Behavior and Mechanical Properties. *J. Biomater. Sci., Polym. Ed.* **2008**, *19*, 1503–1520.
26. Tong, X.; Zheng, J. G.; Lu, Y. C.; Zhang, Z. F.; Cheng, H. M. Swelling and Mechanical Behaviors of Carbon Nanotube/Poly(vinyl alcohol) Hybrid Hydrogels. *Mater. Lett.* **2007**, *61*, 1704–1706.
27. Yang, Z. H.; Cao, Z.; Sun, H.; Li, Y. Composite Films Based on Aligned Carbon Nanotube Arrays and a Poly(*N*-isopropyl acrylamide) Hydrogel. *Adv. Mater.* **2008**, *20*, 2201–2205.
28. Wu, S. N.; Li, H.; Chen, J. P.; Lam, K. Y. Modeling Investigation of Hydrogel Volume Transition. *Macromol. Theory Simul.* **2004**, *13*, 13–29.
29. Gartstein, Y. N.; Zakhidov, A. A.; Baughman, R. H. Mechanical and Electromechanical Coupling in Carbon Nanotube Distortions *Phys. Rev. B* **2003**, *68*, 115415.
30. Yang, L.; Han, J. Electronic Structure of Deformed Carbon Nanotubes. *Phys. Rev. Lett.* **2000**, *85*, 154–157.
31. Leeuw, T. K.; Tsyboulski, D. A.; Nikolaev, P. N.; Bachilo, S. M.; Arepalli, S.; Weisman, R. B. Strain Measurements on Individual Single-Walled Carbon Nanotubes in a Polymer Host: Structure-Dependent Spectral Shifts and Load Transfer. *Nano Lett.* **2008**, *8*, 826–831.
32. Choi, J. H.; Strano, M. S. Solvatochromism in Single-Walled Carbon Nanotubes *Appl. Phys. Lett.* **2007**, *90*, 223114.
33. Walsh, A. G.; Vamivakas, A. N.; Yin, Y.; Cronin, S. B.; Unlu, M. S.; Goldberg, B. B.; Swan, A. K. Screening of Excitons in Single, Suspended Carbon Nanotubes. *Nano Lett.* **2007**, *7*, 1485–1488.
34. Arnold, M. S.; Green, A. A.; Hulvat, J. F.; Stupp, S. I.; Hersam, M. C. Sorting Carbon Nanotubes by Electronic Structure Using Density Differentiation. *Nat. Nanotechnol.* **2006**, *1*, 60–65.
35. Mansur, H. S.; Sadahira, C. M.; Souza, A. N.; Mansur, A. A. P. FTIR Spectroscopy Characterization of Poly(vinyl alcohol) Hydrogel with Different Hydrolysis Degree and Chemically Crosslinked with Glutaraldehyde. *Mater. Sci. Eng., C* **2008**, *28*, 539–548.
36. Reich, S.; Jantoljak, H.; Thomsen, C. Shear Strain in Carbon Nanotubes under Hydrostatic Pressure. *Phys. Rev. B* **2000**, *61*, R13389–R13392.
37. Cronin, S. B.; Swan, A. K.; Unlu, M. S.; Goldberg, B. B.; Dresselhaus, M. S.; Tinkham, M. Measuring the Uniaxial Strain of Individual Single-Wall Carbon Nanotubes: Resonance Raman Spectra of Atomic-Force-Microscope Modified Single-Wall Nanotubes *Phys. Rev. Lett.* **2004**, *93*, 167401.
38. Tan, P. H.; Rozhin, A. G.; Hasan, T.; Hu, P.; Scardaci, V.; Milne, W. I.; Ferrari, A. C. Photoluminescence Spectroscopy of Carbon Nanotube Bundles: Evidence for Exciton Energy Transfer *Phys. Rev. Lett.* **2007**, *99*, 137402.

39. Torrens, O. N.; Milkie, D. E.; Zheng, M.; Kikkawa, J. M. Photoluminescence from Intertube Carrier Migration in Single-Walled Carbon Nanotube Bundles. *Nano Lett.* **2006**, *6*, 2864–2867.
40. Capaz, R. B.; Spataru, C. D.; Tangney, P.; Cohen, M. L.; Louie, S. G. Hydrostatic Pressure Effects on the Structural and Electronic Properties of Carbon Nanotubes. *Phys. Status Solidi B* **2004**, *241*, 3352–3359.
41. Dresselhaus, M. S.; Dresselhaus, G.; Saito, R.; Jorio, A. Exciton Photophysics of Carbon Nanotubes. *Annu. Rev. Phys. Chem.* **2007**, *58*, 719–747.
42. Perebeinos, V.; Tersoff, J.; Avouris, Ph. Scaling of Excitons in Carbon Nanotubes *Phys. Rev. Lett.* **2004**, *92*, 257402.
43. Capaz, R. B.; Spataru, C. D.; Ismail-Beigi, S.; Louie, S. G. Diameter and Chirality Dependence of Exciton Properties in Carbon Nanotubes *Phys. Rev. B* **2006**, *74*, 121401.
44. Dukovic, G.; Wang, F.; Song, D. H.; Sfeir, M. Y.; Heinz, T. F.; Brus, L. E. Structural Dependence of Excitonic Optical Transitions and Band-Gap Energies in Carbon Nanotubes. *Nano Lett.* **2005**, *5*, 2314–2318.
45. Selim, M. S.; Seoudi, R.; Shabaka, A. A. Polymer Based Films Embedded with High Content of Znse Nanoparticles. *Mater. Lett.* **2005**, *59*, 2650–2654.